Science Signaling
AAAS

www.sciencesignaling.org/cgi/content/full/8/386/ra72/DC1

Supplementary Materials for

Protein phosphatase 2A regulatory subunit B56α limits phosphatase activity in the heart

Sean C. Little, Jerry Curran, Michael A. Makara, Crystal F. Kline, Hsiang-Ting Ho, Zhaobin Xu, Xiangqiong Wu, Iuliia Polina, Hassan Musa, Allison M. Meadows, Cynthia A. Carnes, Brandon J. Biesiadecki, Jonathan P. Davis, Noah Weisleder, Sandor Györke, Xander H. Wehrens, Thomas J. Hund, Peter J. Mohler*

*Corresponding author. E-mail: peter.mohler@osumc.edu

Published 21 July 2015, *Sci. Signal.* **8**, ra72 (2015)
DOI: 10.1126/scisignal.aaa5876

The PDF file includes:

Figure S1

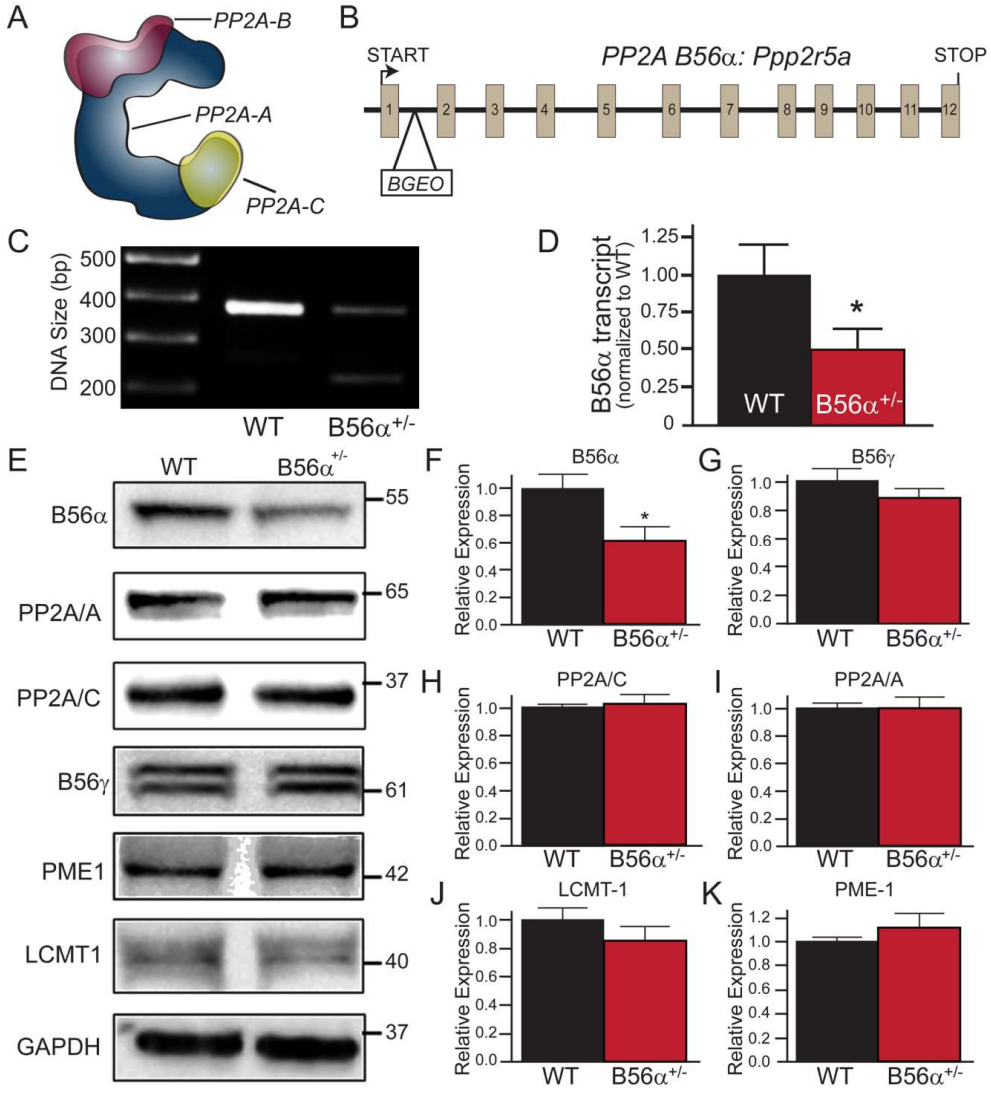

Fig. S1. B56α$^{+/-}$ mice display reduced B56α abundance without changes in the abundance of PP2A core subunits. (A) The PP2A holoenzyme is comprised of structural (*PP2A-A*), regulatory (*PP2A-B*), and catalytic (*PP2A-C*) subunits. *(B)* Scheme for *Ppp2r5a* animal model. *(C)* Representative genotyping of wild-type and B56α$^{+/-}$ mice. *(D)* PCR validation *Ppp2r5a* abundance in wild-type and B56α$^{+/-}$ hearts (n=3 hearts/genotype; *p<0.05). (E) Representative immunoblots of PP2A-related proteins in wild-type and B56α$^{+/-}$ heart lysates. (F-K) Abundance of PP2A subunits and regulatory enzymes in wild-type and B56α$^{+/-}$ mouse hearts; *p<0.05 compared to wild-type; n=6 hearts/genotype.

Figure S2

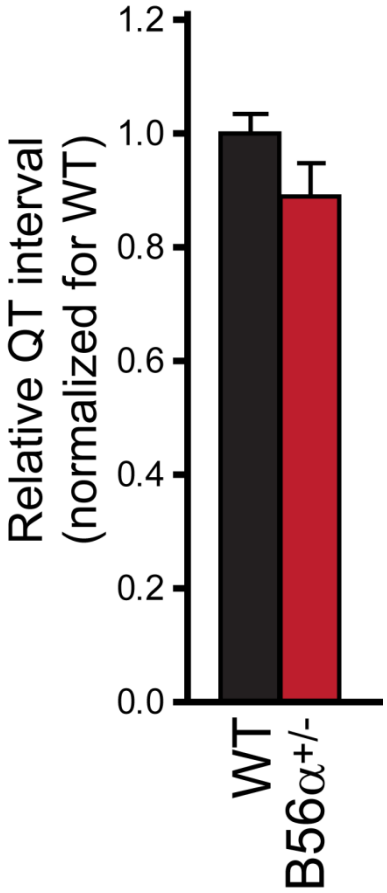

Fig. S2. Wild-type and B56α$^{+/-}$ mice have similar QT intervals. Relative QT interval of conscious wild-type and B56α$^{+/-}$ mice averaged over a 24 hour period; n=4 mice/genotype; p=N.S.

Figure S3

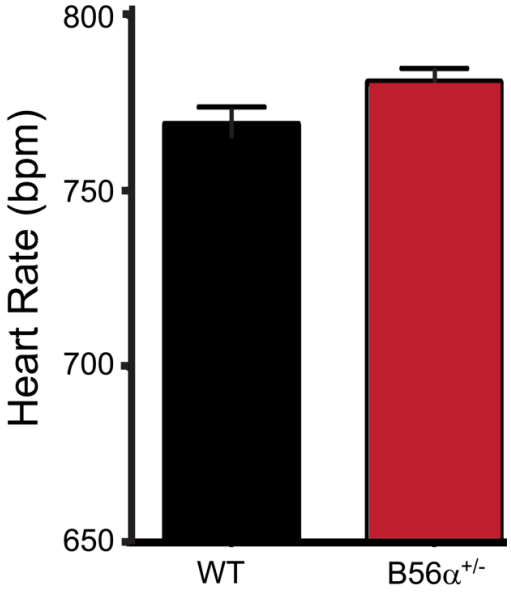

Fig. S3. Wild-type and B56α$^{+/-}$ mice have similar peak heart rates after exercise. Quantification of heart rate of conscious wild-type and B56α $^{+/-}$ mice following strenuous exercise protocol; n=4 mice/genotype; p=N.S.

Figure S4

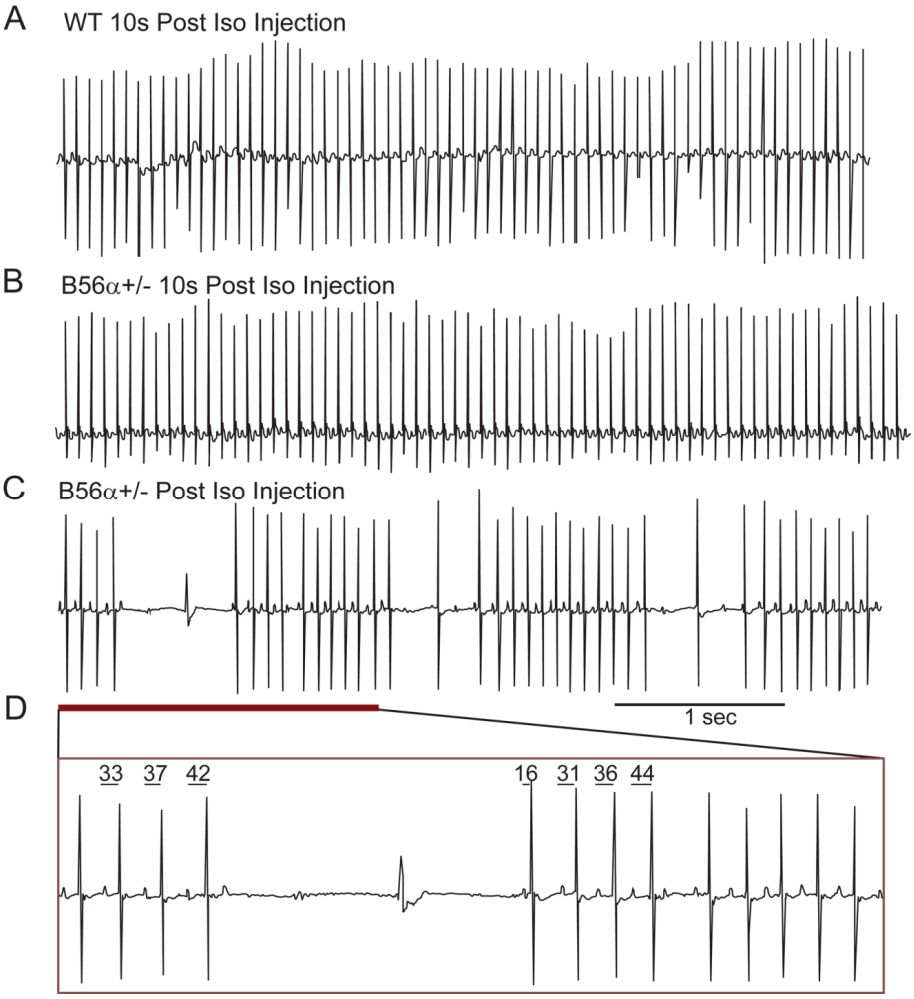

Fig. S4. B56α$^{+/-}$ mice display an aberrant response to adrenergic stimulation. (A-B) Representative wild-type and B56α$^{+/-}$ ECG traces 10 s post Iso injection. (*C*) Reduced heart rate in B56α$^{+/-}$ mice post Iso was associated with sinoatrial (SA) and atrio-ventricular (AV) node dysfunction. (*D*) Iso-dependent arrhythmias in B56α $^{+/-}$ mice are characterized by progressive PR interval prolongation (numbers above PR interval indicate msec) followed by a dropped QRS complex in addition to the lack of continuous P-waves. Phenotypes shown in *(A-D)* were consistently observed in 3 mice/genotype.

Figure S5

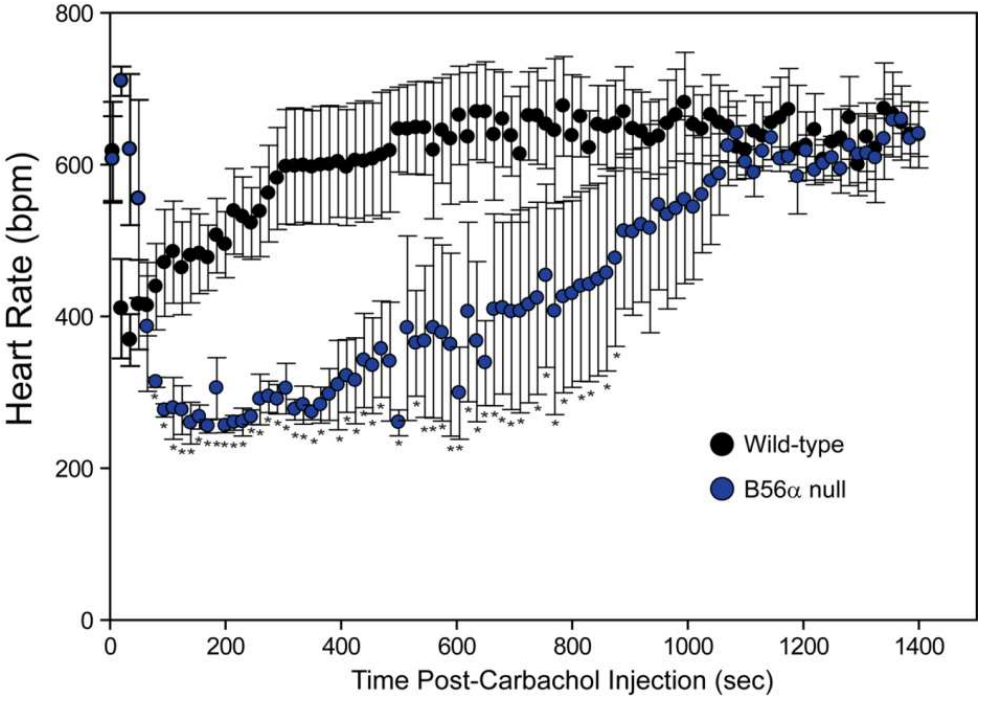

Fig. S5. B56α$^{-/-}$ mice display phenotypes associated with increased parasympathetic activity. Following acetylcholine receptor activation (CCH; 0.1 mg/kg), B56α$^{-/-}$ mice displayed a more pronounced reduction in heart rate compared to wild-type mice. Data represents n=3 mice/genotype (*p<0.05 compared to wild-type).

Figure S6

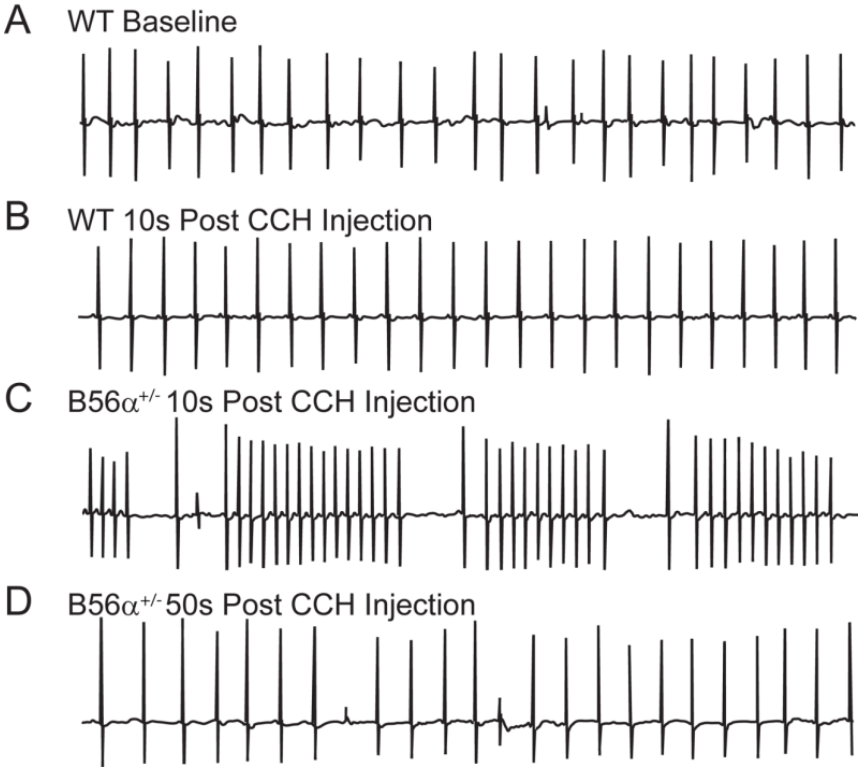

Fig. S6. B56α$^{+/-}$ mice display exaggerated cholinergic response to carbachol administration. Following acetylcholine receptor activation with carbachol (0.1 mg/kg), B56α$^{+/-}$ mice displayed a more pronounced reduction in heart rate compared to wild-type mice. (*A-B*) Representative wild-type ECG traces at baseline and post carbachol (CCH) show normal slowing of heart rate with minor RR interval variability. (*C-D*) B56α$^{+/-}$ mice post CCH injection initially present with SA and AV node dysfunction that continued >50s following injection. All ECG traces shown are 5s in duration and represent data from n=3 mice/genotype.

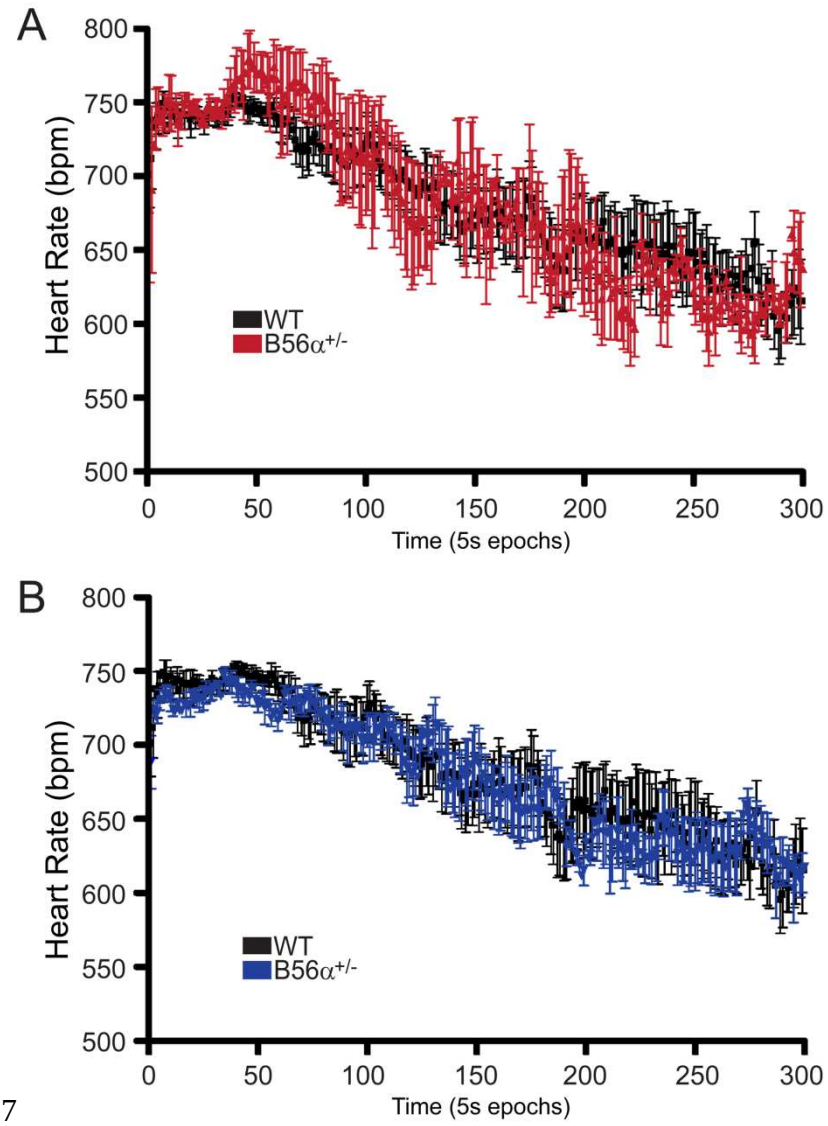

Figure S7

Fig. S7. B56α$^{+/-}$ and B56α$^{-/-}$ mice display normal ECG responses after inhibition of muscarinic acetylcholine receptors. (A-C) Wild-type, B56α$^{+/-}$ and B56α$^{-/-}$ mice displayed similar heart rate response following injection of atropine (1 mg/kg). Wild-type, B56α$^{+/-}$, and B56α$^{-/-}$ mice did not present with either atrial or ventricular arrhythmias. Data represents data from n=3 mice/genotype (p=N.S.).

Figure S8

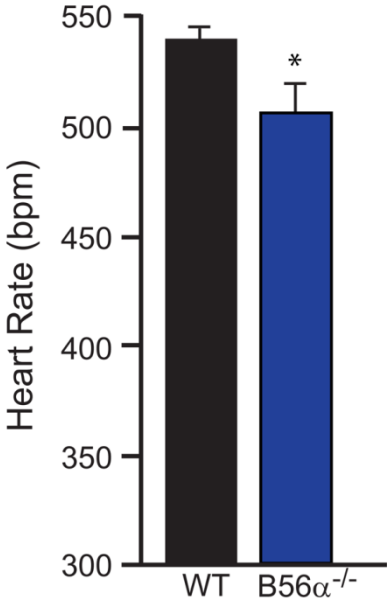

Fig. S8. B56α-deficient mice display reduced heart rate after inhibition of sympathetic and parasympathetic signaling. B56α deficient mice display reduced heart rate compared with wild-type mice following injection of atropine plus propranolol (n=3 mice/genotype; *$p<0.05$ compared with wild-type).

Figure S9

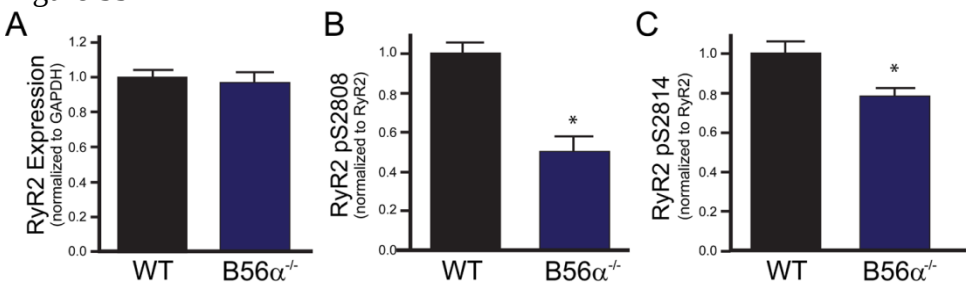

Fig. S9. B56α$^{-/-}$ hearts display reduced phosphorylation of RyR$_2$. *(A-C)* Quantification of proteins from wild-type and B56α$^{-/-}$ heart lysates. *(A)* Although total RyR$_2$ abundance was unchanged, B56α$^{-/-}$ mice showed reduced phosphorylation of RyR$_2$ at *(B)* Ser^{2808} or *(C)* Ser^{2814} (abundance normalized to total RyR$_2$ abundance). For all experiments, n=4 hearts/genotype; *p<0.05.

Figure S10

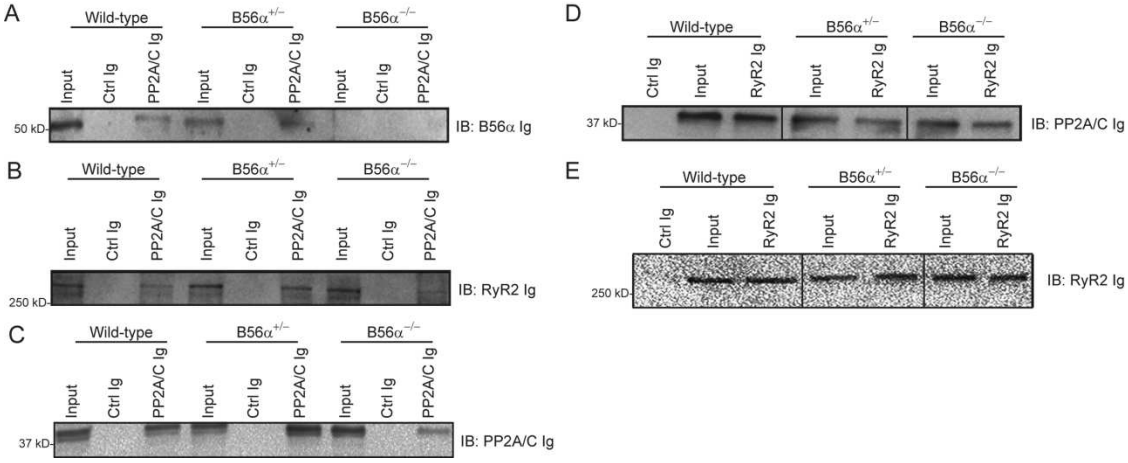

Fig. S10. B56α associates with PP2A/C and RyR_2 but is not required for the interaction between RyR_2 and PP2A/C. (*A*) B56α co-immunoprecipitates with PP2A/C from cardiac lysates from wild-type hearts. As expected, B56α did not co-immunoprecipitate with PP2A/C from B56$\alpha^{-/-}$ hearts. (*B*) PP2A/C and RyR_2 co-immunoprecipitate (using PP2A/C Ig) in wild-type, B56$\alpha^{+/-}$, and B56$\alpha^{-/-}$ hearts. *(C)* Control experiments illustrating PP2A/C in co-immunoprecipitations from *B*. (*D*) PP2A/C and RyR_2 co-immunoprecipitate (using RyR_2 Ig) in wild-type, B56$\alpha^{+/-}$, and B56$\alpha^{-/-}$ hearts. *(E)* Control experiments illustrating RyR_2 in co-immunoprecipitations from *D*. Biochemical data was replicated in three independent experiments using three hearts/genotype.

Figure S11

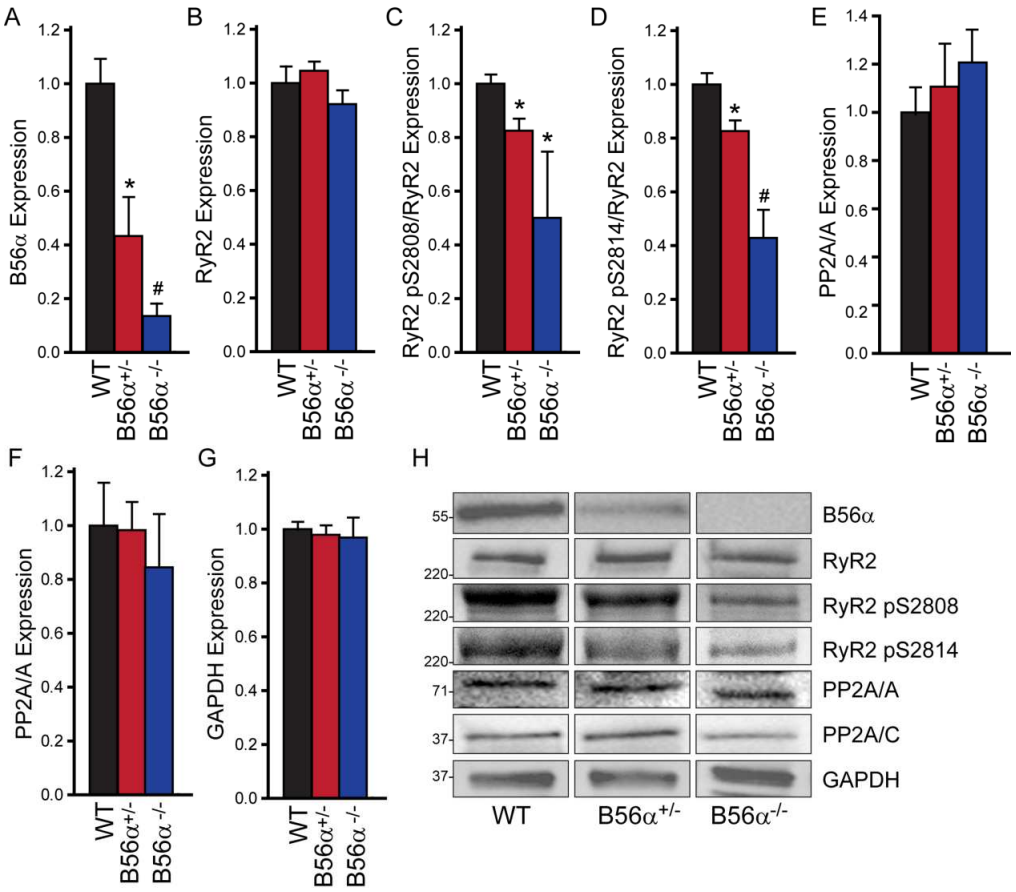

Fig. S11. B56α$^{+/-}$ and B56α$^{-/-}$ atria display reduced phosphorylation of RyR$_2$. (A-G) Quantification of B56α, RyR$_2$ and PP2A proteins from wild-type, B56α$^{+/-}$, and B56α$^{-/-}$ atrial lysates (*p<0.05). *(B)* Although total RyR$_2$ abundance was unchanged, B56α$^{+/-}$ and B56α$^{-/-}$ atria showed reduced phosphorylation of *(C-D)* RyR$_2$ phosphorylated at Ser^{2808} or Ser^{2814} (phosphorylation was normalized to total RyR$_2$ abundance; *p<0.05). We observed no significant difference in the abundance of PP2A/A, PP2A/C, or GAPDH between wild-type, B56α$^{+/-}$, and B56α$^{-/-}$ atrial lysates (p=N.S.). *(H)* Representative immunoblots for experiments in *A-G*. For all experiments, n=3 atria/genotype.

Figure S12

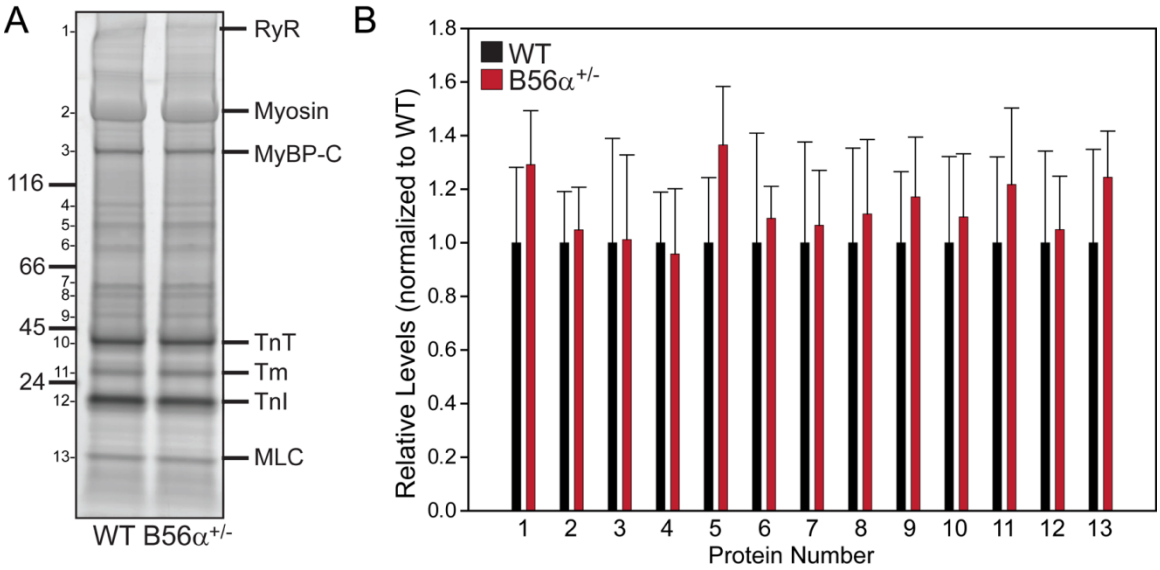

Figure S12. Myofilament proteins are phosphorylated to a similar extent in wild-type and B56α$^{+/-}$ mice. (A) Representative ProQ stain (representative of n=3 mice/genotype) for total protein phosphorylation levels of myofilament proteins compared between wild-type and B56α$^{+/-}$ whole tissue lysates. *(B)* Relative levels of phosphorylation in cardiac proteins from wild-type (n=3) and B56α$^{+/-}$ heart lysates (n=3 hearts/genotype; p= N.S. for all thirteen proteins analyzed). Protein numbers in *B* (1-13) represent bands on blot in panel *A*.

Figure S13

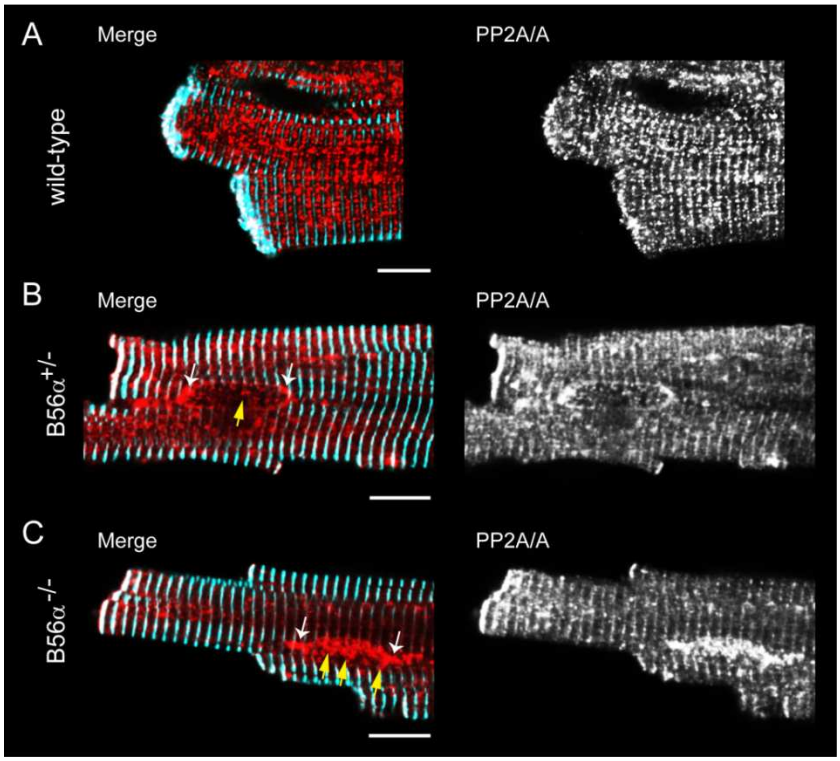

Fig. S13. The PP2A core enzyme is differentially localized in B56$\alpha^{+/-}$ and B56$\alpha^{-/-}$ myocytes. In wild-type myocytes, PP2A/A (red left, white right) is distributed across myocyte membranes and cytosol. In contrast, both B56α $^{+/-}$ and B56$\alpha^{-/-}$ myocytes display increased perinuclear (white arrows) and nuclear (yellow arrows) distribution of PP2A/A. However, PP2A is still found in cytosol and on membranes of B56$\alpha^{+/-}$ and B56$\alpha^{-/-}$ myocytes. Scale bar equals ten microns, blue represents alpha-actinin labeling. Images are representative of >10 myocytes analyzed per mouse from three mice per genotype.

Figure S14

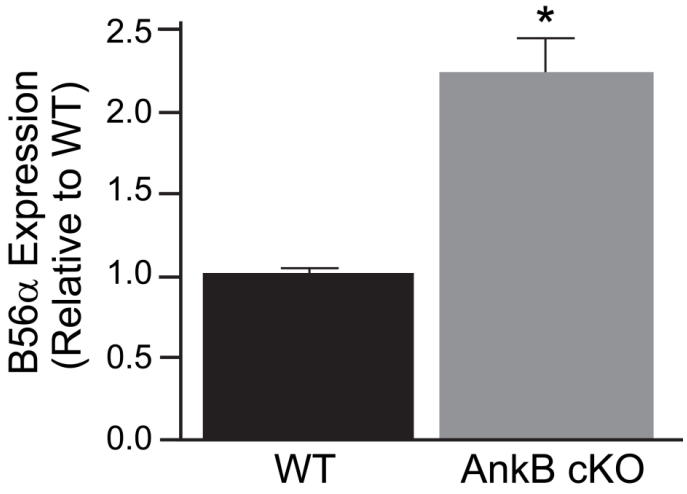

Fig. S14. B56α abundance is increased in ankyrin-B–deficient hearts. αMHC-Cre; *Ank2*$^{f/f}$ mouse (AnkB cKO) cardiac lysates display increased abundance of B56α compared with wild-type heart lysates (n=3 cardiac lysate preparations/genotype, *****p□0.05).